Caldera faults capture and deflect inclined sheets: An alternative mechanism of ring-dike formation

John Browning[1*] and Agust Gudmundsson[1]

[1]*Department of Earth Sciences, Royal Holloway, University of London, Egham TW20 0EX*

E-mail: john.browning.2012@rhul.ac.uk

ABSTRACT

The sub-surface structures of caldera ring-faults are often inferred from numerical and analogue models as well as from geophysical studies. All of these inferred structures need to be compared with actual ring-faults so as to test the model implications. Here we present field evidence of magma channeling into a caldera ring-fault as exhibited at Hafnarfjall, a deeply eroded and well exposed 5 Ma extinct volcano in Western Iceland. At the time of collapse caldera formation, over 200 m of vertical displacement was accommodated along a ring-fault, which is exceptionally well exposed at a depth of approximately 1.2 km below the original surface of the volcano. There are abrupt changes in the ring-fault attitude with depth, but its overall dip is steeply inward. Several inclined sheets within the caldera became arrested at the ring-fault; other sheets became deflected up along the fault to form a multiple ring-dike. We present numerical models showing stress fields that encourage sheet deflection into the sub-vertical ring-fault. Our findings provide an alternative mechanical explanation for magma channeling along caldera ring-faults, which is a process likely to be fundamental in controlling the location of post-caldera volcanism.

INTRODUCTION

Many ring-faults around the world are intruded by dikes (e.g. Smith and Bailey, 1968; Johnson et al, 2002). These dikes are believed to have been emplaced either during the injection of magma during collapse caldera formation (Anderson, 1936; Sparks, 1988; Walter, 2008) or incrementally through many injections along the ring-fault (Saunders, 2001). The common assumption, based on Anderson's (1936) model, is that ring-dikes are injected directly into the ring-fault at its contact with the magma chamber.

Dikes and sheets commonly intrude pre-existing weaknesses such as joints (Delaney et al, 1986) and faults (Gudmundsson, 2011; Magee et al., 2013; Bedard et al, 2012). Whilst there are numerous examples of well-studied ring-faults, for example Glencoe caldera (Clough et al., 1909; Kokelaar, 2007) and Hannegan caldera (Tucker et al., 2007) as well as many others (see Lipman, 1984); observations of well-exposed ring-faults and ring-dikes in the same vertical cross section at depth are extremely rare. As such, the mechanics of magmatic interaction with caldera faults is still poorly understood.

Many calderas experience post-collapse resurgence which may culminate in eruptive activity. Commonly, post-caldera volcanism concentrates spatially above the vertical extent of a caldera ring-fault (Geyer and Marti, 2008; Saunders, 2004). Therefore, understanding the sub-surface structure of caldera ring-faults is important for identifying the location and timing of renewed volcanic activity within active calderas. Caldera ring-faults have traditionally been studied using analogue (e.g Acocella et al., 2000; Acocella, 2007; Geyer et al., 2006; Holohan et al., 2005;

Kennedy et al., 2004), numerical (e.g Gudmundsson, 1998; Hardy, 2008), and analytical methods (e.g Gudmundsson, 1998), with the sub-surface structure often inferred from such models, as well as from seismicity (e.g Ekstrom, 1994), geodetic studies (e.g Jonsson, 2009) and near-surface observations (e.g Geshi et al., 2002; Troll and Walter, 2002). Caldera ring-faults are primarily sub-vertical dip-slip shear fractures, although in some cases the faults accommodate oblique slip (Holohan et al., 2013). Whether a caldera ring-fault dips inward or outward from the center of subsidence is a long debated and contentious issue (Gudmundsson and Nilsen, 2006; Burchardt and Walter, 2010; Geyer and Marti, 2014). For example, Branney (1995) suggests that most ring-faults dip outward, whereas observations from the collapse of Miyakejima, Japan in 2000 (Geshi et al, 2002; Burchardt and Walter, 2010) and Piton de la Fournaise, La Reunion in 2007 (Michon et al, 2009) indicate both inward and outward-dipping ring-faults. The use of near surface observations of ring-faults (e.g., Michon et al, 2009) may be misleading as caldera walls are subject to mass-wasting and erosion (Lipman, 1997). Furthermore, it may be difficult to infer correctly the sub-surface structure from surface observations because the fault-generating local stresses are likely to vary with depth in the volcanic edifice, thereby affecting the overall geometry of the fault structure (Gudmundsson, 2011).

Here we present field data and numerical models which show that dikes and sheets can become deflected at and along a ring-fault, the deflection being primarily due to the difference in material properties between (and within) the fault zone and the host rock. These observations and associated modeling provide an alternative mechanism for the formation of ring-dikes.
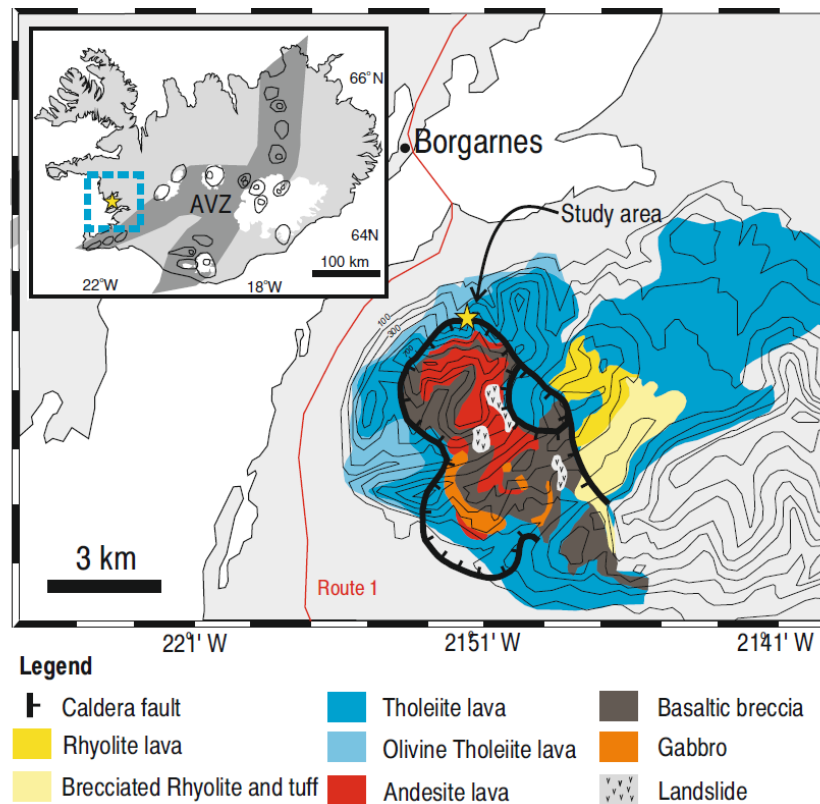
Figure 1. Geological map of Hafnarfjall central volcano, located in Western Iceland, approximately 50 km northwest of the active volcanic zone (AVZ). The ring-fault of the 7.5 × 5 km NW – SE elongated caldera is shown. Study area is marked with a yellow star. Modified after Franzson (1978).

A WELL EXPOSED CALDERA RING-FAULT IN WESTERN ICELAND

Hafnarfjall is an inactive and deeply eroded 5 Ma old central volcano (stratovolcano with a caldera) in Western Iceland. The volcano is comprised of a predominantly basaltic lava pile overlain by brecciated andesite and andesitic lava, as described in detail by Franzson (1978) (Fig. 1). The volcano originally formed in the southwest volcanic zone of Iceland, but subsequently

drifted, through crustal spreading, 40-50 km (Gautneb et al., 1989) to the west-northwest of the rift zone. Hafnarfjall therefore offers the opportunity to study a caldera formed in a divergent plate boundary setting. We estimate that glacial erosion has removed the uppermost parts of the volcano based on the assumptions of Walker (1960) and Johannesson (1975) who used zonation of amygdale minerals to estimate the level of erosion in a nearby area. Hafnarfjall volcano contains numerous inclined sheets, predominantly basaltic, which dip on average at around 65°, trend NE, and have thicknesses that are commonly about 1 m or less (Gautneb et al., 1989). The thickest sheets, however, reach about 10 m and tend to be composed of rhyolite. Many of these intrusions in Hafnarfjall are highly altered, and it is often difficult to discern characteristic intrusive features such as chilled selvages and cooling jointing. In Figure 2 we show several dikes and inclined sheets ranging in thickness from 2.5 m (Fig. 2a) to 3 cm (Fig. 2c). They are all clearly intrusions which are discordant to bedding, however very few display characteristic chilled selvages or discernable horizontal fracture patterns.
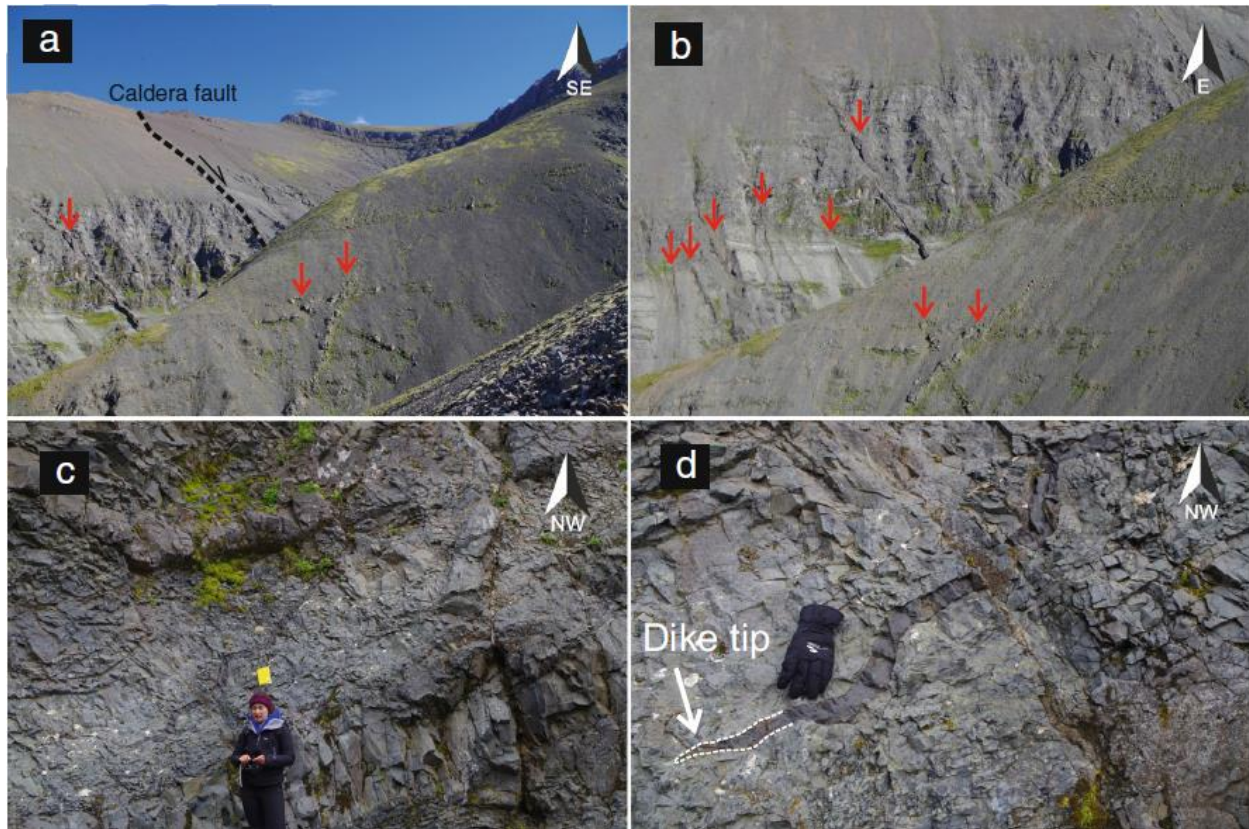
Figure 2. Examples of sheets and dikes found in the Hafnarfjall lava pile. A) View southeast towards the caldera ring-fault, indicated as a dashed line. B) Dikes and sheets are discernable as discordant linear features within the lava pile, in this example a pair of cross-cutting dikes, the largest and youngest of which is approximately 2.5 m in thickness and dips 65-75°S. Other dikes and sheets are indicated by red arrows. C and D) a 3 cm thick arrested dike exhibiting a narrow and pointed dike tip, due to weathering and alteration it is difficult to observe any chilled selvage or horizontal fracture pattern within the dike; this is common in many of the intrusions in Hafnarfjall.

At around 4.6 Ma, Hafnarfjall experienced a major collapse event, forming part of a NW-SE elongated caldera approximately 7.5 × 5 km in diameter (Franzson, 1978). The most striking evidence of this collapse is the exposed ring-fault in a gulley, oriented roughly NW-SE, at the northernmost margin of the caldera, as shown in Figure 3. At this locality, an E-W trending segment of the ring-fault can be observed in vertical cross-section for 200 m along dip and

around 700 m along strike (Fig. 3a). Here the ring-fault cuts a 300 m thick lava pile composed of 2–5 m thick flows of basaltic tholeiite. Around the outer caldera margin lavas dip 15° S, whereas the dip of lavas which constitute the caldera block increase to ~35° S. This implies that the caldera block has tilted during faulting. Dips of intra-caldera lavas also increase with depth towards the center of the caldera, i.e. individual lava layers at the outcrop base exhibit a steeper dip than those near the present day surface. The caldera fault can be traced in several localities as mapped by Franzson (1978) and shown in Figure 1 as a single fault plane with displacement in excess of 100 m. The exposure described in detail here indicates a throw in excess of 200 m, although the normal fault offset is considered a minimum and is based on the inability to trace individual lava flow layers horizontally, across the entire vertical section. As mentioned, the vertical section is 300 m, although individual lava layers can only be obviously discerned for approximately 200 m of this section.

The studied vertical section of ring-fault does not display a constant attitude. This finding is in contrast to those of many models on ring-fault formation that often predict a simple inward- or outward-dipping trend (Acocella, 2007). Instead, the fault alternates in dip between 85 N – 90° and 85 S – 90° , suggesting that a number of stress perturbations occurred during fracture propagation. Such subtle changes in fault attitude are unlikely to be detected in models unless a heterogeneous, in particular, a layered, edifice is considered. On average the fault has a normal trend and dips steeply inward, at ~85°S.

Steep-sided slopes surrounding the fault exposure limit observations to the base of two gullies and, from distance, to a parallel topographic high (Fig. 3, a&b). At the base of the caldera fault
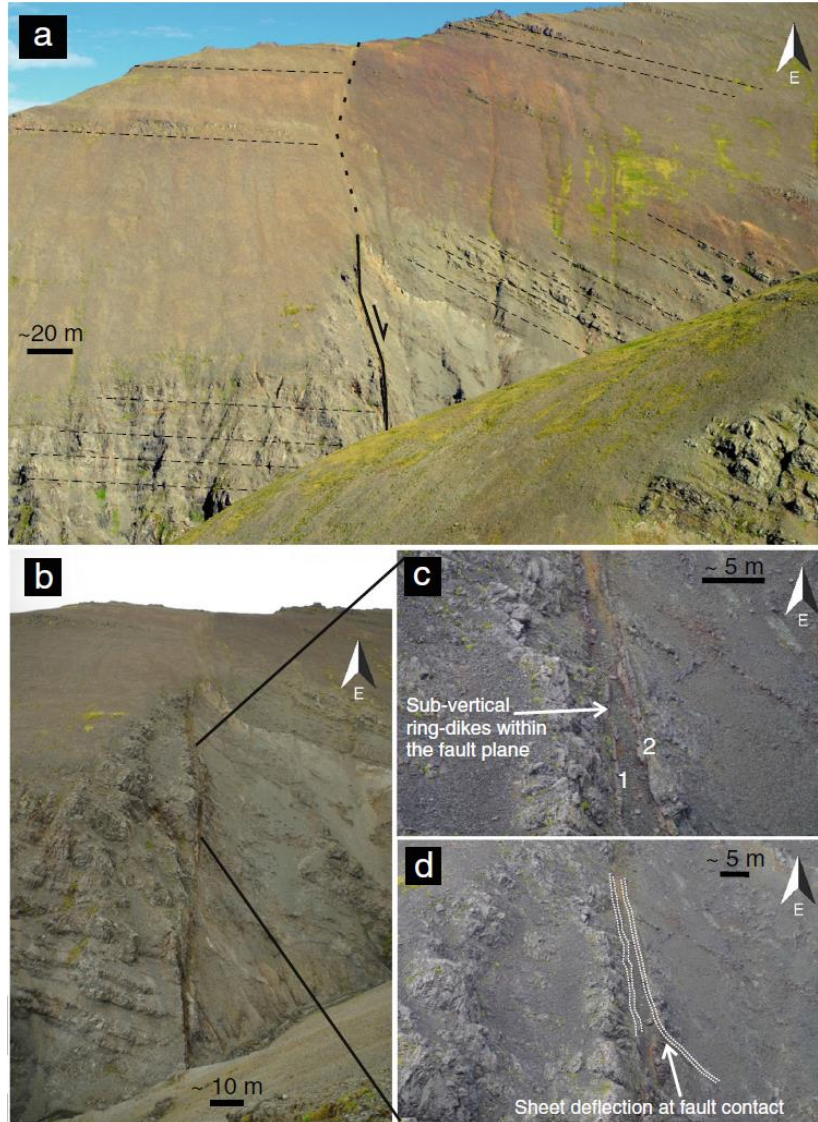
Figure 3. A). Caldera ring-fault exhibits a general inward dipping normal trend, although subtle variations in attitude occur throughout. The height from the base to the top of the fault is ~300 m. Lavas on the inner caldera margin dip more steeply than those outside, and generally dip increases with depth. Several markers are used to infer synclinal drag folding, perhaps the most prominent is a light white tuff which clearly bends into the fault. Displacement is greater than the vertical section, so no horizontal markers can be traced across the fault plane. B) Many individual lava layers with thicknesses between 1 and 2 m can be traced to the fault contact on the outer margin, however most lavas on the inner margin are sufficiently deformed and not discernable. C and D) Section of the upper observable part of the fault. Individual dikes shown and numbered are around 1 m thick. (Location 64°30'01" N 21°52'39" W)

(Fig. 4) are five thin (< 0.7 m) basaltic, but highly altered, dikes. Thin (0.5-1 cm) mineral veins separate some of the individual intrusions, as shown in Figure 4c. Surprisingly, no breccia or fault gouge is found along the main fault plane. We interpret the dikes within the fault plane as ring-dikes, and now refer to them as such throughout. In Figure 4b, two ring-dikes can be clearly observed within the fault plane, the northern most dike strikes N086°E, it becomes offset around 25 m vertically in the pile. The strike of the second dike is variable between approximately 095 and 115 and appears to follow the fault plane. In the intra-caldera lava pile, thin (< 1 m) inclined sheets dip between 45-75°S, and upon contact with the fault, the sheets either become arrested or change attitude and deflect vertically into the fault. No sheets can be traced from inside of the caldera margin, across the fault, and to the outside of the caldera.

On the intra-caldera margin, synclinal drag folding indicates a normal sense of dip-slip shear and displacement, see Figure 3a. The zone of folding extends for approximately 10-15 m horizontally toward the caldera center. In this region it is difficult to distinguish between individual lava flows, as their characteristic scoria margins have been sufficiently deformed. There is no indication of reverse sense displacement or motion on the fault, which is a commonly interpreted mechanism during caldera unrest due to magma intrusion (Acocella et al., 2000; Walter and Troll, 2001; Jonsson, 2009). This is important to note, as our later numerical models simulate an over-pressured condition, which is of course a requirement for propagating the original sheets described throughout.
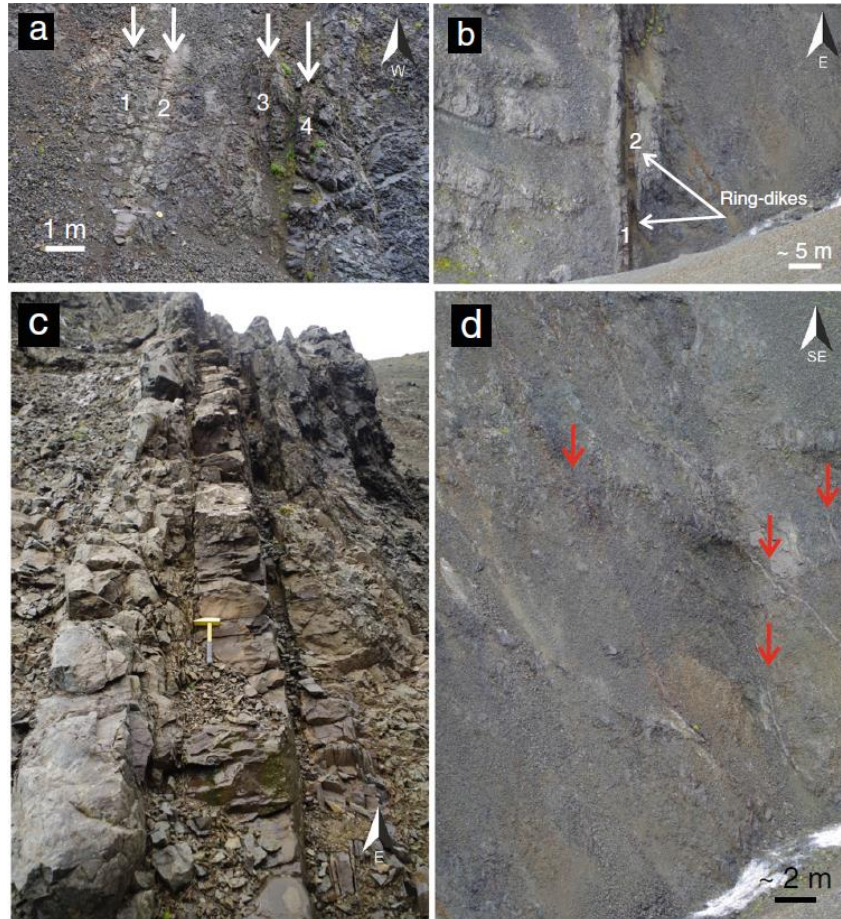
Figure 4. Base of the outcrop of the ring-fault; where four thin ring-dikes (< 0.7 m) of basaltic composition occupy the sub-vertical segment. Two of these dikes are observable in the vertical section (B), one can be traced for approximately 25 m before it becomes arrested, the other continues through the entire fault length. Inside the caldera margin (D) several inclined sheets strike E-W to NE-SW and dip between 65-80° S, at least two of the sheets meet the fault contact higher in the pile.

FACTORS INFLUENCING THE PROPAGATION OF DIKES AND SHEETS

Stress barriers

In order for a sheet to successfully propagate, tensile stress magnitudes should exceed the *in situ* host rock tensile strength, which is generally between 0.5-6 MPa (Amadei and Stephansson, 1997; Gudmundsson, 2011). The direction of propagation is based on Anderson's (1936) theory

of sheet and ring-dike propagation and on numerous field observations of dikes and sheets which suggest that magmatic fractures will propagate in a direction parallel to the trajectories σ_1 and perpendicular (or normal) to σ_3 (cf. Gudmundsson, 2011). A stress barrier is a layer or unit where the local stress field is unfavorable for the propagation of a particular type of fracture. For example, for a vertically propagating extension fracture, a stress barrier would be a layer where the maximum compressive stress flips to horizontal, a situation which favors dike arrest (Gudmundsson and Phillip, 2006). Both stiff (high Young' modulus) and soft (low Young's modulus, compliant) layers can act as stress barriers (Gudmundsson and Phillip, 2006).
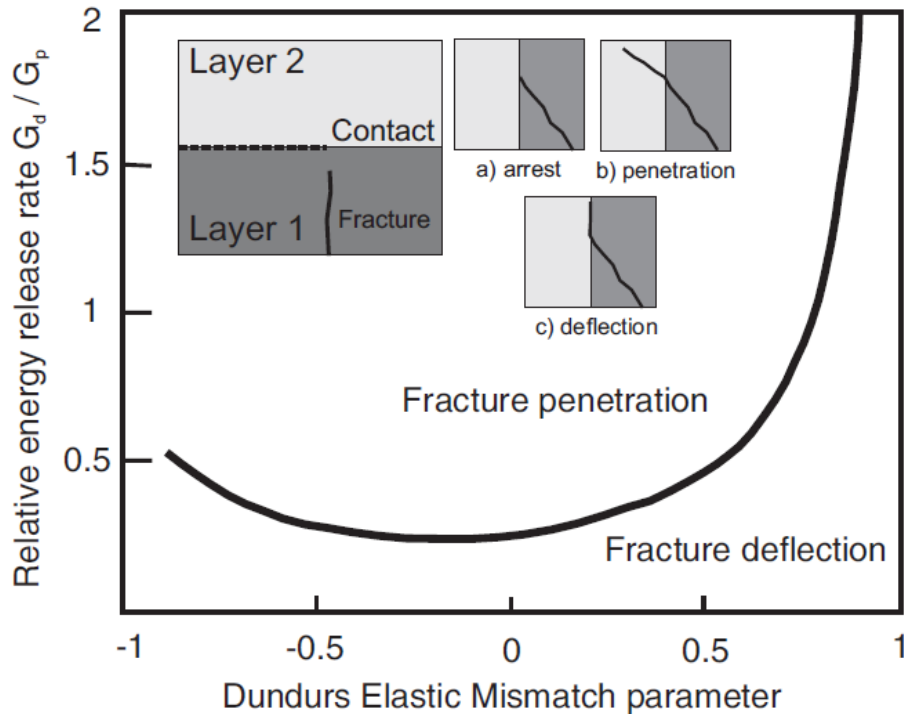

Figure 5. Conditions for fracture propagation: upon meeting a contact between two layers with contrasting material properties, a fracture will either a) arrest, b) penetrate the contact or c) deflect at the contact. The ratio of strain energy release rate for fracture deflection (G_d) against fracture penetration (G_p) is plotted as a function of the Dundurs elastic mismatch parameter (α), see text for details. Modified after He et al. (1994)

Elastic mismatch

The second mechanism responsible for dike deflection is related to the difference in material properties of the layers hosting, and directly in front of, a propagating fracture and the associated contacts. Dikes and sheets are extension fractures or mode I cracks. However, when such fractures meet and become deflected into a contact or discontinuity they temporarily become mixed-mode (He and Hutchinson, 1989; Xu et al., 2003). Consider the total strain energy release rate G_{total} in mixed-mode fracture propagation:

$$G_{total} = G_I + G_{II} + G_{III} = \frac{(1-v^2)K_I{}^2}{E} + \frac{(1-v2)K_{II}{}^2}{E} + \frac{(1+v)K_{III}{}^2}{E} \qquad (1)$$

G_{I-III} are energy release rates (Jm^{-2}) of ideal mode I-III cracks (Anderson, 2005; Gudmundsson, 2011), E is Young's modulus, v is Poisson's ratio, and K_{I-III} are stress intensity factors. When the rock layer which hosts the dike or sheet has the same or similar mechanical properties to a rock layer above, then the strain energy release rate for a mode I crack, G_p, reaches a value suitable for fracture extension, which is equal to the material toughness of the layer, Γ_L. Therefore, from Eq. (1) the condition becomes:

$$G_p = \frac{(1-v^2)K_I{}^2}{E} = \Gamma_L \qquad (2)$$

However, the dike or sheet will deflect into the discontinuity if the strain energy release rate becomes the same as the material toughness of the discontinuity, Γ_D. Deflection at the discontinuity then occurs when:

$$G_d = \frac{(1-v^2)}{E}(K_I{}^2 + K_{II}{}^2) = \Gamma_D \qquad (3)$$

It follows that a dike or sheet will continue on the same trajectory, through a discontinuity if (He and Hutchinson, 1989):

$$\frac{G_d}{G_p} < \frac{\Gamma_D(\Psi)}{\Gamma_L} \qquad (4)$$

Or become deflected at the discontinuity if:

$$\frac{G_d}{G_p} \geq \frac{\Gamma_D(\Psi)}{\Gamma_L} \qquad (5)$$

Where Ψ denotes the measure of the relative proportion of mode II to mode I:

$$\Psi = \tan^{-1}(K_{II} / K_I) \qquad (6)$$

In Figure 5, the ratio of G_d/G_p is plotted as a function of α, which represents the Dundurs elastic mismatch parameter and can be presented in the following form (He and Hutchinson, 1989):

$$\alpha = \frac{E_1 - E_2}{E_1 + E_2} \qquad (7)$$

Here E denotes the plain-strain Young's modulus, and the subscripts 1 and 2 relate to the moduli of the rock above and hosting the dike, respectively. The ratio below the curve in Figure 5 indicates areas where the deflection of a dike or sheet is favored, whereas those areas above the curve indicate continued propagation with no deflection.

Cook-Gordon mechanism

Experiments on crack propagation have shown that Cook-Gordon debonding is a common mechanism in the delamination of composite materials (Xu et al., 2003; Wang and Zu, 2006). It has been shown that the tensile strength ahead of a propagating dike can open up a contact ahead of the dyke tip (Gudmundsson, 2011). Such a mechanism is important in where there is an abrupt change in the mechanical properties or rocks across an interface or a contact, particularly when the contact is clearly defined and mechanically weak (with a low tensile strength). However in a fault zone such as that described previously, the contact between the fault and host rock is not clearly defined. As such, we do not consider this mechanism as important for capturing sheets within the fault, at least initially.

NUMERICAL MODEL SETUP

To test the proposal that sheets can become arrested at, or deflected into a caldera fault, we made several numerical models. In all the models, we calculate the stress field around a 1 m thick dike subject to an internal magmatic excess pressure of 5 or 10 MPa as the initial loading. The weight of overlying host rock, or the overburden pressure is included in the lithostatic stress (Jaeger and

Cook, 1979), and is therefore taken into account when considering loading as excess pressure in the sheet (Gudmundsson, 2011).
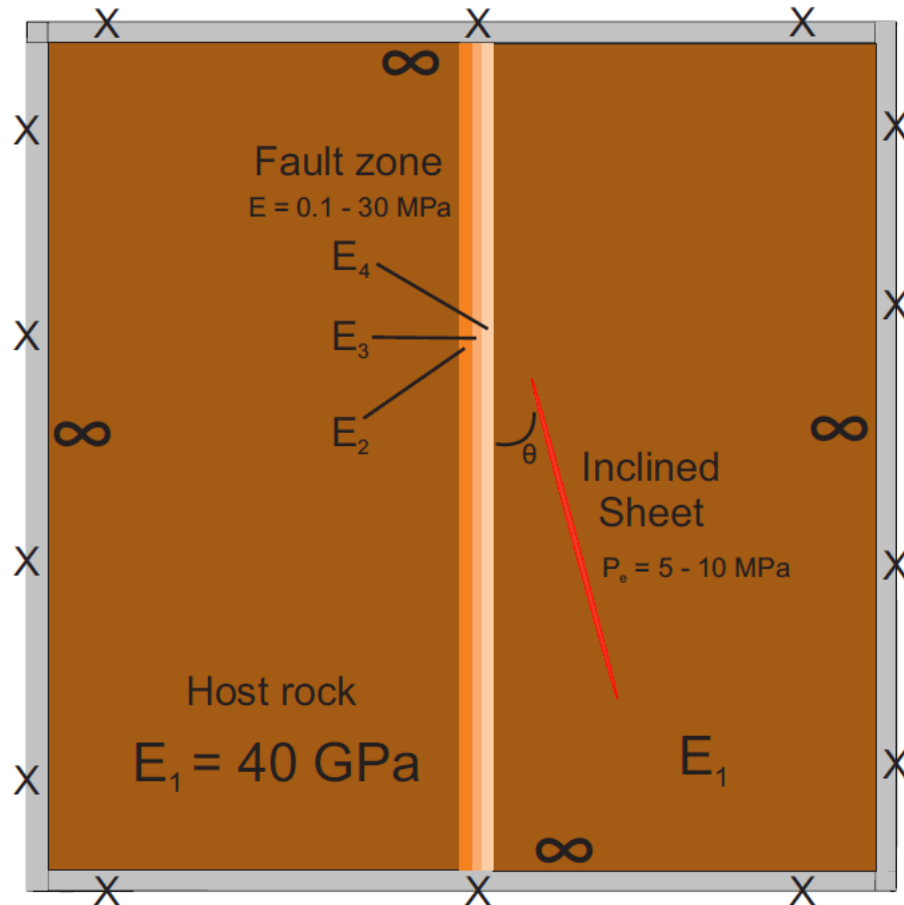

Figure 6. General COMSOL model setup used throughout. In all runs the models are fastened at the outer boundary using a fixed constraint, this is coupled with an infinite element domain on the inner model margin to ensure the fixed boundary effects do not influence results. The host rock and fault zone are modelled using different values for Young's modulus (E) as specified in the results section. An inclined sheet is modelled as a cavity with an excess pressure (P_e), sheet angle is varied throughout model runs.

In the numerical models presented here (Fig. 7-11), the focus is on the mechanical properties of the caldera fault zone, namely the stiffness or Young's modulus (*E*) of the layers that constitute the damage zone and the core of the fault, and the more gently dipping layers through which the sheet propagates. Density and Poisson's ratio is kept constant in all model runs, with values of

2500 kg m^{-3} and 0.25 respectively. We estimate that the damage zone surrounding the ring-fault is approximately 15 m thick, and occurs predominantly on the southern, down-throw ('hanging wall') side of the fault. The damage zone is qualitatively estimated based on the ability to discern individual lava flows, which on the northern wall can be traced to the fault contact, but on the southern wall are highly altered and deformed. This deformation zone is observed laterally south for around 15 m from the fault core, which contains the ring-dikes, to a point where individual lava flow characteristics are discernible. Fault core and damage zones have been recognized and measured on different scales in many areas of Iceland (Gudmundsson, 2005). The fault zone is modelled simply as three individual layers of similar thickness, but with differing mechanical properties. The models presented are designed to test how the local stress field changes as an inclined sheet a) approaches a ring-fault and b) becomes captured by the fault.

The sheet is situated perpendicular to the fault zone, see the model setup in Figure 6. A section of ring-fault is modeled in two dimensions as a series of sub-vertical layers decreasing in stiffness towards a fault core, replicating the variation in stiffness of the fault damage zone (e.g., Gudmundsson, 2011). In this setup, the softest layer is the fault core which is characterized by the lowest value of Young's modulus or stiffness (0.1 GPa), this is surrounded by a fault damage zone which stiffens gradually approaching that of the host rock (40 GPa). For simplicity, here the damage-zone stiffness is assumed constant at any particular time. Fault zone stiffness, however, was varied over time in separate model runs to incorporate the dynamic nature of fault development both syn- and post-collapse. Temporal changes reflect initial fault growth, and subsequent healing and intrusion by dikes. All models simulate snapshots of the magnitudes and directions of principal stress around the pressurized sheet; the likely propagation path is then

inferred based on the trajectories of the maximum principal compressive stress (σ_1). Boundary conditions were used to test the model's response to a simulated vertical normal-fault dip-slip displacement (Fig. 11), modeled as a compressive stress, of 5 MPa applied to the collapsing block, and normal-fault dilation (Fig. 11), modeled as a tensile stress, of 5 MPa applied perpendicular to the fault. Trajectories of the maximum principal compressive stress (σ_1) and the magnitude of the minimum principal compressive stress (σ_3) are shown in all model runs.

MODEL RESULTS

Several numerical models were run with different fault zone set-ups, generated by varying the mechanical properties (Young's modulus) across the fault. A homogeneous setting, whereby the fault zone shared the same mechanical properties as the host rock was initially modelled, and provided a reference to compare other model results. In this setup the fault has little or no effect on sheet propagation. Additional model runs are displayed throughout, Figures 7-11.

Several geometrical set-ups were run by varying sheet dip angle (θ), to confirm the relative effects of fault zone mechanical heterogeneity against intrusion angle. We observe that shallow dipping sheets, those with dips less than 45°; do not alter the local fault stress significantly enough to promote deflection or arrest, unless additional boundary conditions are applied, see Fig 11. In all models the maximum tensile stress (σ_3) occurs at the sheet tip, and the maximum compressive stress (σ_1), shown as white cones, are used to interpret the likely fracture pathway. All models show stress contours in the range of 0.5-6 MPa, the upper end of this range being the most likely to induce fracturing (Amadei and Stephansson, 1997).
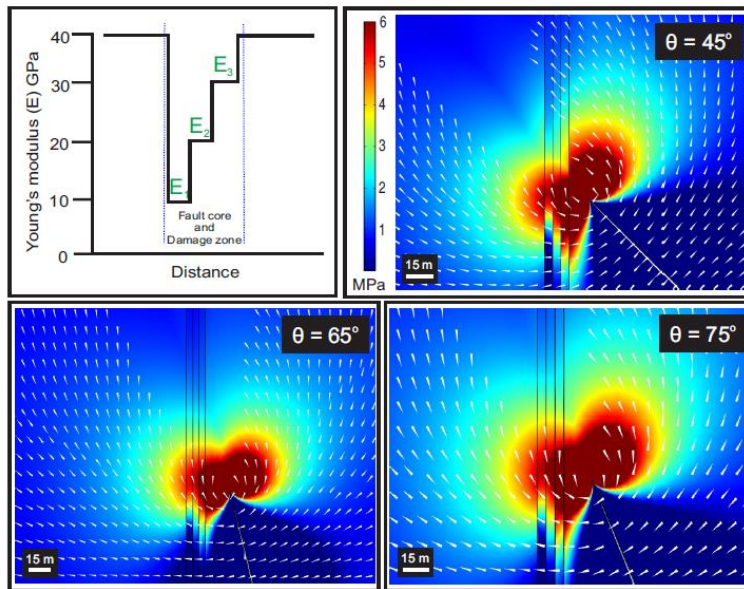
Figure 7. Young's modulus in the fault zone ranges between 10-30 GPa. Sheet dips shown are 45°, 65° and 75°, and sheet overpressure is 10 MPa. In all models tensile stress concentrates through the fault plane, indicating that any fracture would likely propagate through the fault. Rotation of the maximum principal compressive (white cones) occurs in line with fault dip for those sheets that dip 65° and greater, suggesting that a fracture may align preferentially with the fault. Large stress shadows are created ahead of fracture tip, as indicated by absence of stress trajectories.
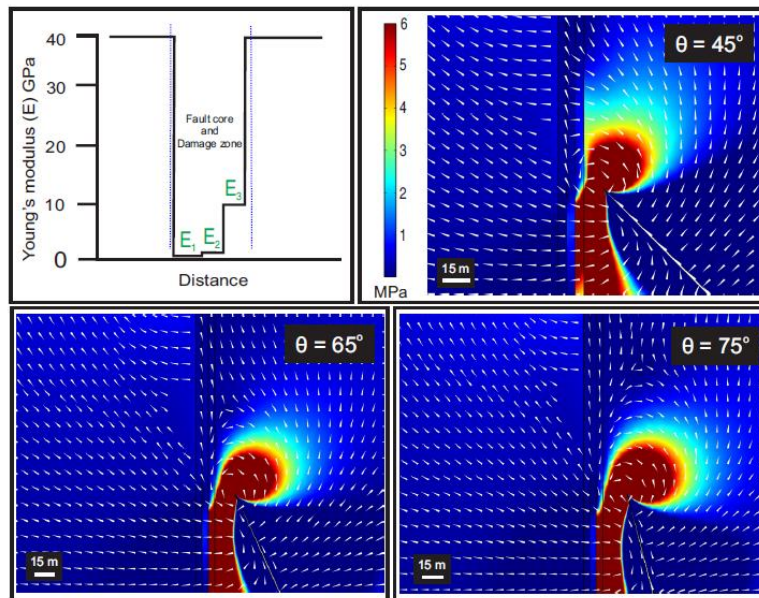

Figure 8. Young's modulus in the fault zone ranges between 0.1-10 GPa, sheet overpressure is 10 MPa in all models. In all model runs, tensile stress concentrates within the 10 GPa layer closest the sheet. Softer layers suppress most of the tensile stress, and principal stress rotation within the fault core favors vertical sheet deflection. This rotation effect is much less pronounced

for those sheets which dip below 60-70°, for example the 65° model shown displays inclined σ₁ trajectories throughout the vertical fault cross-section.
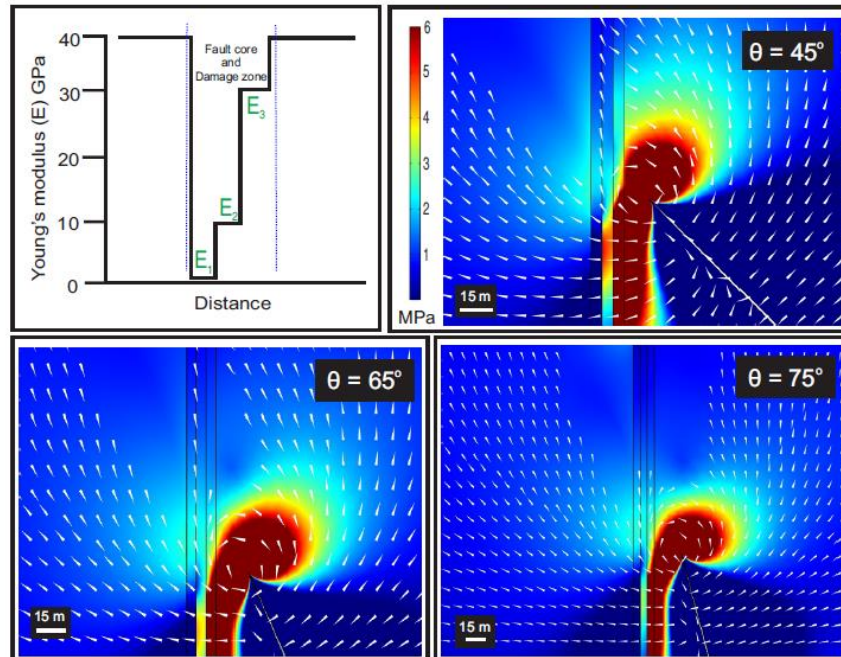

Figure 9. Fault zone Young's modulus ranges from 1-30 GPa, sheet overpressure is 10 MPa in all models. In models with sheets that dip greater than ~45°, a significant rotation of the maximum compressive stress is observed. In C and D the trajectories of σ₁ rotate to vertical within the fault, whereas in B trajectories are initially vertical but become inclined higher up the fault.

When a mechanical contrast between the fault and host rock is modeled, a rotation of principal stress occurs near the sheet tip and a temporary change in principal stress orientation at the contact between the fault and host rock. In order for the sheet to become deflected into a sub-vertical dike along the ring-fault, as observed in Hafnarfjall, the values of Young's modulus must be sufficiently different between the individual modeled fault zone layers, in order to induce an elastic mismatch. Figure 7 highlights a situation whereby the layers which constitute the fault damage zone are not significantly different from those of the host rock and thus promote neither elastic mismatch nor principal stress rotation. This condition, namely similar elastic properties of

the fault zone and the host rock, favors transverse sheet propagation through the fault. In contrast

models shown in Figures 8 and 9, simulate a more mechanically heterogeneous fault zone, with

Young's modulus differing by orders of magnitude. In these situations sheet deflection is favored

due to the mechanical mismatch between the individual layers. The fracture propagation path at

the sheet tip is inferred from the trajectories of σ_1 (which the sheet follows), surrounding the

sheet and fault zone. It is only when these trajectories rotate to sub-vertical that the sheet will

deflect into a dike within the fault. Such a situation is much more likely in models which

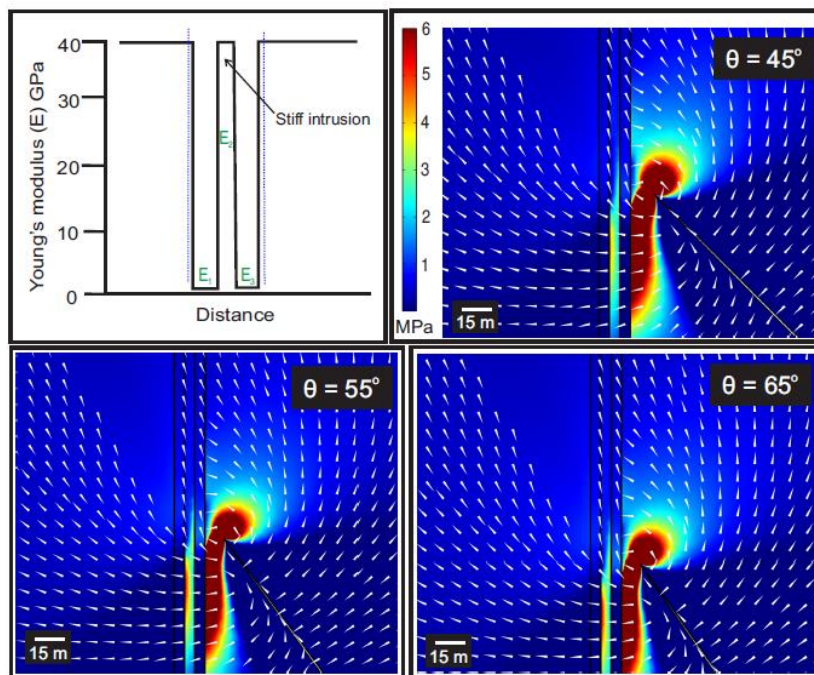simulate a sheet with an initially steep dip (i.e >65°).

Figure 10. A stiff layer (40 GPa) is added to the center of the fault zone to simulate a previous dike intrusion. Principal stress rotation at the sheet tip and stress concentration within the stiff layer, favors fault capture, most likely along the nearside edge of the previous intrusion. Sheet approach angle has little effect on the stresses within the fault zone above 35°.
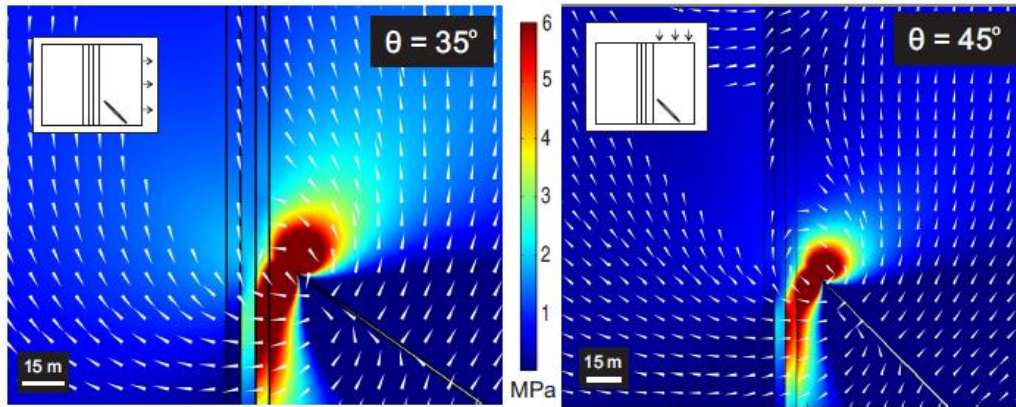
Figure 11. Models showing the effect of various boundary conditions, here a tensile stress (5 MPa) is applied to the far right of model (a) and a compressive stress (5 MPa) to the upper part of the intra-caldera block in model (b).

To model the effect of a previously intruded dike in the ring-fault, a stiff layer is added to the center of the fault zone (Fig.10). Such a situation is likely if a lower part of the fault was intruded by a ring-dike in the conventional manner described by Anderson (1936) and Walter (2008), or if inclined sheets were previously captured and deflected (see appendix 1). The stiff layer creates a clear stress barrier and zone of elastic mismatch, indicating that transverse sheet propagation in this scenario is unlikely. Instead any sheet would likely become deflected or arrested at the contact between the weak damage zone and the stiff dike, (Fig. 10).

Boundary conditions were applied to the models edge to simulate 1) extension across the fault and 2) block subsidence. A compressional stress of 5 MPa was applied to the intra-caldera block (Fig. 11). In this model run, the modeled principal stress axis rotates to sub-vertical with little dependence on the angle of the sheet, this situation would favor sheet propagation into and along the plane of the ring-fault, thereby allowing magma to propagate in a manner consistent with that interpreted from field observations, although principal stress rotation further up dip of the fault may induce fracture arrest later on. The second boundary condition simulates an extensional

force acting perpendicular to the fault, which would likely encourage fault dilation. In these situations it is much easier for a low angle sheet to deflect into the fault; in Figure 11 we show a 35° dipping sheet.
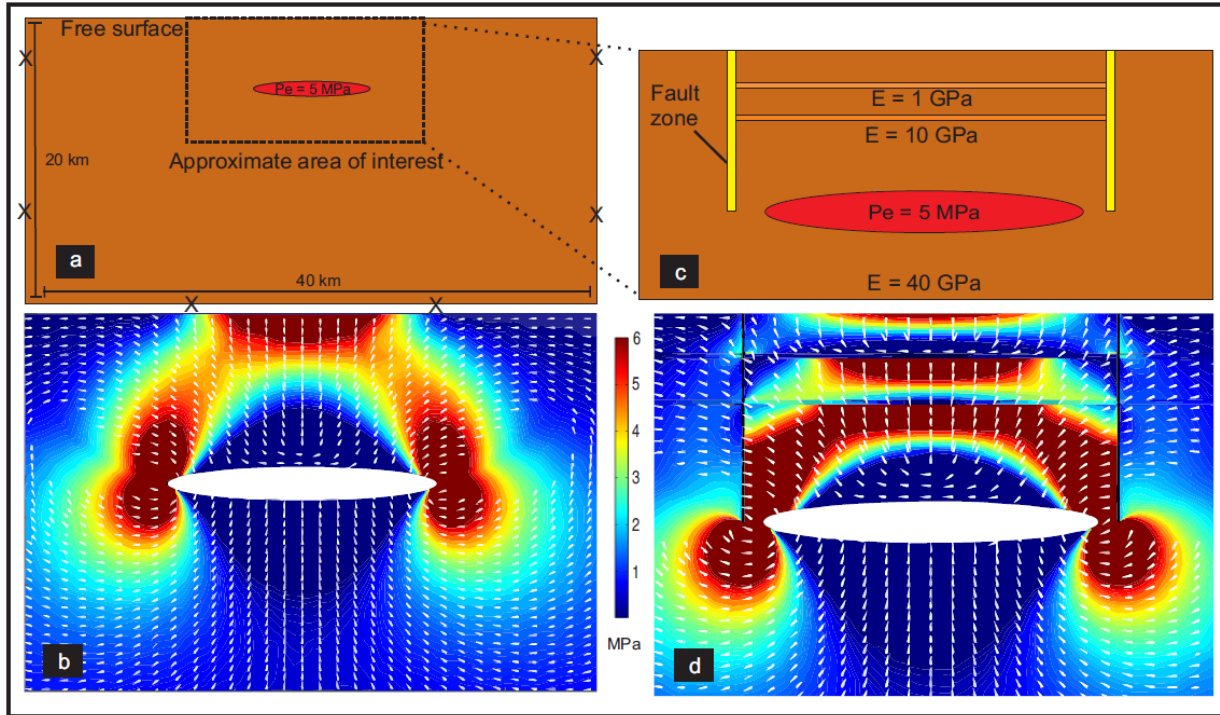

Figure 12. Background stresses associated with a modelled A) 8 km wide and 1 km thick sill like magma chamber at 5 km depth with an overpressure of 5 MPa. B) Principle stresses become oriented in manner which favors inclined sheet propagation from the chamber margins. C) Model setup includes a peripheral fault zone, with a lower Young's modulus than the surrounding host rock, as well as two soft horizontal layers at 1 and 2 km depth. D) Results indicate that the fault acts as a significant stress barrier. Furthermore the soft horizontal layers act in a similar manner, also exhibiting significant principle stress rotation at the boundary of the upper most, and softest layer.

Finally a model is included to assess the background boundary effects of a magma chamber subject to pressure in excess of lithostatic, a necessary requirement for the propagation of a sheet. In this model (Fig. 12) an 8 km wide and 1 km thick sill like magma chamber is situated in a homogeneous crustal segment at 5 km depth. The magnitude and orientation of stresses highlight the potential for inclined sheet propagation, particularly at the chambers outer margins.

Several softer layers were added to the model, these were placed vertically to simulate the caldera fault zones previously discussed, and horizontally to simulate, in a simple way, mechanical layering in a volcanic edifice. Stresses clearly concentrate within the fault margins in the caldera block, indicating that faults act as stress barriers. There is little principle stress rotation observed at the fault contact, indicating that if the tensile stress was high enough ($0.5 - 6$ MPa) to generate a fracture then the likely propagation path would be through the fault. However, the required stress concentration is rarely met as the inner (core) part of fault tends to suppress stresses.

Once a fault captures an inclined sheet and deflects it into the first sub-vertical dike, it is generally much easier for subsequent sheets to deflect at the contact between the lava pile and the first dike (Fig. 3). This follows because the stiffness of a vertical intrusion is much greater than that of the area surrounding the fault damage zone, and therefore principal stress rotation and elastic mismatch parameters favor dike propagation over continuation of an inclined sheet.

DISCUSSION AND CONCLUSIONS

It is well known that normal faults can alter the propagation pathway of sub-vertical dikes (Valentine and Krogh, 2006; Gaffney et al, 2007; Ziv and Rubin, 2000) and sills (Magee et al, 2013). Several assumptions and inferences have been made regarding the role of caldera ring-faults in channeling magma (Anderson, 1936; Saunders, 2011; Jonsson, 2009); the most common mechanical explanation offered to decipher this process relies on magma chamber underpressure (Anderson, 1936). This model suggests that many ring-dikes form during large explosive eruptions, leading to chamber-roof collapse, and the flow of evolved magmas up into the ring-

faults. Alternative mechanical models are hampered by the poor availability of data on the structure of ring-faults at depth, and the lack of detailed observations of the interactions between ring-faults and magma.

Here we present an alternative mechanism of ring-dike formation which suggests that some ring-dikes do not channel magma directly from the margins of a magma chamber, but rather form through inclined sheets being captured and deflected along the ring-fault (Fig. 13). This mechanism is in agreement with observations of restless calderas (e.g Saunders, 2001) and the location of numerous dike fed eruptive centers, located on ring-fault margins (Walker, 1984; Geyer and Marti, 2008). However, several caldera volcanoes experience eruptive activity located outside of their ring-fault margins, for example the fissure eruptions of Fernandina in 1995 (Chadwick et al., 2011). Our model supports the interpretation that the sheet which fed these fissures had a shallow dip (12-14°) at a depth of ~1 km; near the chamber margin (Chadwick et al., 2011). This follows because sheet deflection is unlikely at dip angles lower than ~45°, see Figures 7-10. Note, also, that many mafic calderas have complex ring-fault structures controlled by post-collapse subsidence, for example Colli Albani (Giordano et al, 2006).

Dikes can become arrested and deflected at contacts between layers with mechanical mismatch (contrasting mechanical properties) such as stiff lava flows and compliant (or soft) tuff layers (Gudmundsson, 2011), see Figure 12. It has been suggested that elastic mismatch and associated local stresses partly control the frequency with which dikes reach the surface to feed eruptions (Gudmundsson and Phillip, 2006). In this view, it is only when the state of stress in a volcanic edifice becomes roughly homogeneous that a dike can propagate to the surface, a condition more

likely to be reached in edifices composed of mechanically similar layers. Similarly, if a caldera fault develops a fault core it may act as a single vertical and roughly homogeneous layer, thereby promoting stress field homogenization and providing a pathway for magma channeling toward the surface.
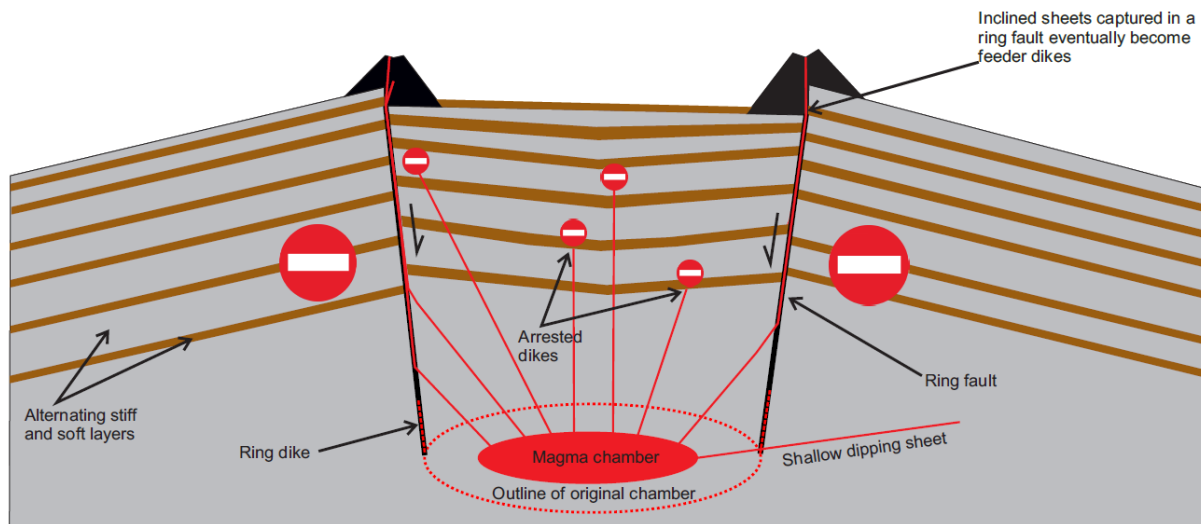

Figure 13. Conceptual resurgent-caldera model. In the model, an edifice is made of layers of contrasting mechanical properties, e.g., stiff lavas and soft tuffs and sediments. A number of dikes fail to reach the surface and become arrested at layer contacts. Inclined sheets propagating from the shallow magma chamber become captured by the ring-fault. The ring-fault deflects many sheets into sub-vertical dikes, some of which may have propagated to the surface. Shallow dipping sheets may penetrate the fault to force eruptions outside of the ring-fault margin.

A large proportion of the world's volcanism occurs within or around active calderas (Newhall and Dzurisin, 1988), and therefore understanding the control of caldera structures on magma movement is vital for predicting the location and timing of eruptive activity. The caldera fault at Hafnarfjall is one of the best exposures of its kind in the world. It represents a segment of the ring-fault, visible as a 200 m vertical exposure. The fault has variable attitude, but overall it is a steeply inward-dipping normal fault.

Many faults offer potential pathways for magma. However, very steeply-dipping faults, such as the ring-fault in Hafnarfjall, are perhaps particularly favored paths because the normal stress on steep faults in rifting environments tends to be comparatively small (Gudmundsson, 2011). In this particular case, the ring-fault has deflected and acted as a channel for inclined sheet propagation; some of the sheets may have reached the surface to supply magma for eruptions. In addition, the ring-fault has captured and deflected inclined sheets to form a ring-dike, a mechanism of ring-dike formation that has not been reported earlier. These results further underline the importance of understanding magma-fault interaction in relation to volcanic hazards. It is likely that the process of sheet deflection and ring-dike formation, described here, provides a major control on the location of resurgent caldera volcanism.

ACKNOWLEDGMENTS

REFERENCES CITED

Acocella V, Cifelli F, Funiciello, R (2000) Analogue models of collapse calderas and resurgent domes. Journal of Volcanology and Geothermal Research 104: 81–96.

Acocella V (2007) Understanding caldera structure and development: An overview of analogue models compared to natural calderas. Earth-Science reviews. 85: 125-160

Amadei B, Stephansson, O (1997) Rock Stress and its Measurement (Chapman and Hall, New York).

Anderson EM (1936) The dynamics and formation of cone-sheets, ring-dikes, and cauldron-subsidence. Royal Society of Edinburgh Proceedings. 128-157

Anderson TL (2005) Fracture Mechanics: Fundamentals and Applications, 3rd ed.
Taylor & Francis, London. 621 pp.

Bedard JH, Naslund HR, Nabelek P, Winpenny A, Hryciuk M, Macdonald W, Hayes, B, Steigerwaldt, K, Hadlari, T, Rainbird R, Dewing K, Girard E (2012). Fault-mediated melt ascent in a Neoproterozoic continental flood basalt province, the Franklin sills, Victoria Island, Canada. Geological society of America Bulletin 124: 723-736

Branney MJ, (1995) Downsag and extension at calderas: new perspectives on collapse geometries from ice-melt, mining, and volcanic subsidence. Bulletin of Volcanology 57: 303-318

Burchardt S. and Walter TR (2010) Propagation, linkage, and interaction of caldera ring-faults: comparison between analogue experiments and caldera collapse at Miyakejima, Japan, in 2000. Bulletin of Volcanology 72: 297–308.

Chadwick WW, Jonsson S, Geist D, Poland M., Johnson DJ, Batt S, Harpp KS, Ruiz A (2011) The May 2005 eruption of Fernandina volcano, Galapagos: The first circumferential dike intrusion observed by GPS and InSAR. Bulletin of Volcanology 73: 679-697.

Clough CTH, Maufe, HB, Bailey EB (1909) The cauldron subsidence of Glen Coe and the associated igneous phenomena. Quarterly Journal of the Geological Society of London 65: 611-678

Delaney PT, Pollard DD, ZIony JI, McKee EH (1986) Field relations between dikes and joints: Emplacement processes and paleostress analysis. Journal of Geophysical Research. 91: 4920-4938

Ekstrom, G (1994) Anomalous earthquakes on volcano ring-fault structures. Earth and Planetary Science Letters 128: 707-712

Franzson H (1978) Structure and petrochemistry of the Hafnarfjall_Skardsheidi central volcano and the surrounding basalt succession, W-Iceland [Ph.D. thesis]: Edinburgh, Scotland, university of Edinburgh 264 pp

Gaffney ES, Damjanac B, Valentine GA (2007) Localization of volcanic activity: 2. Effects of pre-existing structure, Earth and Planetary Science Letters 263: 323–338.

Gautneb H, Gudmundsson A, Oskarsson N (1989) Structure, petrochemistry and evolution of a sheet swarm in an Icelandic central volcano: Geological Magazine 126: 659-673.

Geyer A, Folch A and Martí J (2006), Relationship between caldera collapse and magma chamber withdrawal: An experimental approach, Journal of Volcanology and Geothermal Research 157: 375–386.

Geyer A and Marti J (2014). A short review of our current understanding of the development of ring faults during collapse caldera formation. Front. Earth Sci. 2:22. doi: 10.3389/feart.2014.00022

Geyer A, Martí J (2008) The new worldwide collapse caldera database (CCDB): A tool for studying and understanding caldera processes. Journal of Volcanology and Geothermal Research 175: 334–354.

Geshi N, Shimano T, Chiba T, Nakada S (2002) Caldera collapse during the 2000 eruption of Miyakejima volcano, Japan. Bulletin of Volcanology 64: 55-68

Giordano G, De Benedetti AA, Diana A, Diano G, Gaudioso F, Marasco F, Miceli M, Mollo S, Cas RAF, Funiciello R (2006) The Colli Albani mafic caldera (Roma, Italy): Stratigraphy, structure and petrology. Journal of Volcanology and Geothermal Research 156: 49-80

Gudmundsson A (1998) Formation and development of normal-fault calderas and the initiation of large explosive eruptions. Bulletin of Volcanology 60: 160–170.

Gudmundsson A and Nilsen K (2006), Ring-faults in composite volcanoes: structures, models and stress fields associated with their formation, Geological Society, London, Special Publications 269: 83–108.

Gudmundsson A, Berg SS, Lyslo KB, Skurtveit E (2011) Fracture networks and fluid transport in active fault zones. Journal of Structural Geology 23: 343-353.

Gudmundsson A (2011) Rock fractures in geological processes. Cambridge University Press: Cambridge. doi: 10.1017/CBO9780511975684

Gudmundsson A, Phillip SL (2006) How local stress fields prevent volcanic eruptions. Journal of Volcanology and Geothermal research 158: 257-268

Hardy S (2008) Structural evolution of calderas: Insights from two-dimensional discrete element simulations. Geology 36: 927.

He MY, Hutchinson JW (1989) Crack deflection at an interface between dissimilar elastic materials. International Journal of Solids and Structures. 31: 3443-3455.

He MY, Evans AG, Hutchinson JW (1994) Crack deflection at an interface between dissimilar elastic materials. International Journal of Solids and Structures. 25: 1053-1067

Holohan, EP., Troll, VR., Walter, TR., Münn, S., McDonnell, S. and Shipton, ZK. (2005), Elliptical calderas in active tectonic settings: an experimental approach, Journal of Volcanology and Geothermal Research 144: 119–136.

Holohan, EP., Walter, TR., Schöpfer, MPJ., Walsh, JJ., van Wyk de Vries, B. and Troll, VR. (2013), Origins of Oblique-slip Faulting during Caldera Subsidence, Journal of Geophysical Research: Solid Earth, No. 2, p. n/a–n/a.

Jaeger JC, Cook NGW (1979) Fundamentals of Rock Mechanics. Chapman and Hall, London

Johannesson H (1975) Structure and petrochemistry of the Reykjadalur central volcano and surrounding areas, Midwest Iceland. PhD Thesis, University of Durham, Durham, 273 pp

Johnson SE, Schmidt KL, Tate MC (2002) Ring complexes in the Peninsula Ranges Batholith, Mexico and the USA: magma plumbing systems in the middle and upper crust. Lithos 61: 187-208

Jonsson S (2009) Stress interaction between magma accumulation and trapdoor faulting on Sierra Negra volcano, Galapagos. Tectonophysics 471: 36-44

Kennedy, B., Stix, J., Vallance, JW., Lavallée, Y. and Longpré, MA. (2004), Controls on caldera structure: Results from analogue sandbox modeling, Geological Society of America Bulletin 116: 515.

Kokelaar P (2007) Friction melting, catastrophic dilation and breccia formation along caldera superfaults. Journal of the Geological Society 164: 751-754

Lipman PW (1997) Subsidence of ash-flow calderas: relation to caldera size and magma chamber geometry. Bulletin of volcanology. 59: 198-218

Magee C, Jackson CAL, Schofield N (2013) The influence of normal fault geometry on igneous sill emplacement and morphology. Geology 41: 407–410.

Michon L, Villeneuve N, Catry T, Merle O (2009) How summit calderas collapse on basaltic volcanoes: New insights from the April 2007 caldera collapse of Piton de la Fournaise volcano. Journal of Volcanology and Geothermal Research 184: 138–151.

Newhall, C.G and Dzurisin, D (1988) Historical unrest at large calderas of the world. US Geological survey bulletin. 72, 85-100

Saunders ST (2001) The shallow plumbing system of Rabaul caldera: A partially intruded ring fault? Bulletin of volcanology 63: 406-420

Saunders ST (2004) The possible contribution of circumferential fault intrusion to caldera resurgence. Bulletin of Volcanology 67: 57-71

Smith RL, Bailey RA (1968) Resurgent cauldrons. Geological Society of America Memoirs 116: 613-662

Sparks RSJ (1988) Petrology and geochemistry of the Loch Ba ring-dike, Mull (NW Scotland): an example of the extreme differentiation of theolitic magmas. Contributions to Mineralogy Petrology 100:446-461.

Troll V, Walter TR, Schmincke HU (2002) Cyclic caldera collapse : Piston or piecemeal subsidence? Field and experimental evidence. Geology 30: 135-138, doi:10.1130/0091-7613(2002)030<0135.

Tucker D, Hildreth W, Ullrich T, Friedman R (2007) Geology and complex collapse mechanisms of the 3.72 Ma Hannegan caldera, North Cascades, Washington, USA. Geological Society of America Bulletin 119: 329-342, doi:10.1130/825904.1.

Valentine GA, Krogh KEC (2006) Emplacement of shallow dikes and sills beneath a small basaltic volcanic center – The role of pre-existing structure (Paiute Ridge, southern Nevada, USA), Earth and Planetary Science Letters 246: 217–230.

Walker GPL (1960) Zeolite zones and dike distribution in relation to the structure of the basalts of eastern Iceland. Journal of the Geological Society 68: 515-527

Walker, G. P. L. (1984), Downsag calderas, ring faults, caldera sizes, and incremental growth, Journal of Geophysical Research, 89, 8407-8416

Walter TR (2008) Facilitating dike intrusions into ring-faults. Developments in Volcanology: Caldera volcanism: Analysis, modelling and response 10: 351-374

Walter TR, Troll VR (2011) Formation of caldera periphery faults: an experimental study. Bulletin of Volcanology 63: 191-203

Wang, P. and Xu, L.R. (2006), Dynamic interfacial debonding initiation induced by an incident crack, International Journal of Solids and Structures, Vol. 43 No. 21, pp. 6535–6550.

Xu, L.R., Huang, Y.Y. and Rosakis, A.J. (2003), Dynamic crack de ection and penetration at interfaces in homogeneous materials : experimental studies and model predictions, Vol. 51, pp. 461–486.

Ziv A, Rubin AM (2000) Stability of dike intrusion along pre-existing fractures. Journal of Geophysical Research 105